A DFT mechanistic study of the ODH of n-hexane over isolated H_3VO_4

Nkululeko E. Damoyi[a], Holger B. Friedrich[b], Gert H. Kruger[c], David Willock[d]

[a] Department of Chemistry, Mangosuthu University of Technology, Box 12363, Jacobs, 4026, South Africa
[b] School of Chemistry and Physics, University of KwaZulu-Natal, Westville Campus, Private Bag X 54001, Durban, 4000, South Africa
[c] Catalysis and Peptide Research Unit, School of Pharmacy, University of KwaZulu-Natal, Westville Campus, Private Bag X 54001, Durban, 4000, South Africa
[d] School of Chemistry, Cardiff University, Park Place, Cardiff CF10 3AT, Wales, UK

ARTICLE INFO

Keywords:
DFT
ODH
n-hexane
RDS
Mechanism
Vanadia

ABSTRACT

Catalytic (H_3VO_4) oxidative dehydrogenation (ODH) mechanistic studies of the activation of n-hexane have been conducted by means of Density Functional Theory (DFT).

Catalytic oxidative dehydrogenation is an important strategy for the conversion of alkanes to alkenes to provide useful chemical feedstocks from saturated hydrocarbons. Transition metal oxide catalysts based on vanadium provide an important class of catalysts for this reaction. The catalyst is usually prepared with vana-dium in a high oxidation state prepared as an over layer supported on a relatively inert main group oxide (silica, alumina, etc.). Activation of the hydrocarbon is then energetically possible through the reduction of vanadium cations which can be subsequently re-oxidised using molecular O_2 to complete the catalytic cycle.

The aim of this study was to use density functional theory to explore the catalytic mechanism of this type of reaction using the conversion of n-hexane to 1- and 2-hexene as an illustrative example. Calculations are per-formed for the 1- and 2-hexene radical pathways and the results extrapolated to discuss the expected selectivity under laboratory experimental conditions (573, 673 and 773 K). Consideration of 3-hexene is excluded as in our earlier experimental studies and in the general literature this product is not reported. The stationary points on the potential energy surfaces were characterized and the associated geometries and relative energies ($E^{\#}$, E, $G^{\#}$ and G) were determined. The relative energies of all intermediates and transition states identified are used to lend insight on the mechanistic pathways for the reaction.

We have concentrated on the role of the transition metal in this chemistry and so the catalyst model chosen is an isolated, tetrahedral H_3VO_4 cluster containing one vanadyl bond, V(V)]O. The calculated rate-limiting step is the CeH bond activation (β-hydrogen abstraction) from the C_6H_{14} chain by the vanadyl O, with a calculated $E^{\#}$ = +27.4 kcal/mol. This produces a $C_6H_{13}HOH_3VO_3$ complex as an intermediate with vanadium reduced to V(IV). There are then two possible routes for the propagation step that leads to 2-hexene. Firstly, the abstraction of the second γ-hydrogen on the radical intermediate fragment (%C_6H_{13}) can take place on a different active V (V) = O site. Secondly this step may involve reaction with gas-phase molecular O_2. These alternatives are compared computationally and results used to discuss some existing experimental data.

1. Introduction

Transition metal oxides are frequently used as heterogeneous cata-lysts for oxidation of hydrocarbons to produce a variety of products. Gas phase studies of metal oxide clusters and their reaction behaviour can help to understand the mechanism of elementary reactions in cat-alytic processes under isolated, controlled, and reproducible conditions [1–3].

Vanadium oxide-based catalytic systems are known to be active and selective in many oxidative dehydrogenation (ODH) reactions [4–8]. Studies [9] (Zhanpeisov), [10] (Bronkema, Leo, & Bell) have shown that depending on the method of preparation, vanadium oxide-based cata-lysts possess phases that include isolated VO_4 tetrahedral sites, com-prising one vanadyl bond (V = O), and other phases made up of the dimeric VeOeV species. The V = O bond has been proposed by many investigators to contain a critical oxygen involved in hydrocarbon oxidation reactions [11–15]. Pieck et al. [16] (Pieck, Banares, & Fierro) studied the ODH of propane on V_2O_5/ZrO_2 catalysts and showed that monovanadates have both higher activities and better selectivities to propene than bulk V_2O_5 and polyvanadates. However, generally at high conversions of the alkane, non-selective combustion pathways limit the alkene selectivities, regardless of the good activity for the ODH of

Corresponding author.
E-mail address: damoyi@mut.ac.za (N.E. Damoyi).

alkanes to their corresponding alkenes [17–19]. For example, it is well established that limited propene selectivity at higher propane conver-sions is related to propene adsorption on acid sites and their subsequent combustion to carbon oxides [20] (F. Arena), [21] (Y.-M. Liu). Much effort has been spent over the last decades to develop suitable vana-dium oxide-based catalysts for the oxidative dehydrogenation and se-lective oxidation of light hydrocarbons to valuable olefins and oxyge-nates [22] (E.A. Elkhalifa and H.B. Friedrich), [23] (F. Cavani), however, these processes are still far from industrial application. Earlier experimental studies indicate that the selective oxidation of propane on vanadium oxides proceeds via a Mars–van Krevelen [24] (Mars & Van Krevelen) (redox) mechanism that involves the reduction of the metal oxide surface by the alkane with the formation of the alkene and water, followed by reoxidation of the surface through gas-phase oxygen.

Reactions comprising isolated vanadate species with a variety of support materials including silica, titania and zirconia were previously modelled with a variety of computational methods [25–28]. Reported work on Density Functional Theory (DFT) modelling of catalytic sys-tems and shorter chain hydrocarbons is extensive [29–31], albeit that on long chain alkanes over vanadium oxide-based catalysts is limited. Although heterogeneous catalysis is largely an experimental field, computational modelling and simulation, as a complementary and supplementary tool, is a prominent field that is increasingly being re-cognized as important and essential in the study and development of catalytic systems [32–34]. A good model not only helps experi-mentalists to rationalize their results, but also assist to make predictions that challenge the capability of available experimental techniques in terms of the spatial, time and energy resolutions, and guides experi-mentalists to design new experiments [35] (G.A. Somorjai Y. L., Major successes of theory and experiment-combined studies in surface chemistry and heterogeneous catalysis). Our research group has pub-lished a number of experimental papers involving ODH of n-hexane and higher alkanes over VMgO catalysts [36–39]. The relatively low yields of olefins and aromatics that were obtained in laboratory experiments necessitated this theoretical study. One of the aims of this work was to determine the most active O site, as either the vanadyl O or the bridging O, in n-hexane elementary oxidation reactions to hexenes. The merits of the oxidative dehydrogenation (ODH) conversion of inexpensive al-kanes to produce value added products, such as olefins and aromatics, represents the driving force that motivates the research for developing active and selective catalysts for this purpose [40] (E.A. Elkhalifa, Oxidative dehydrogenation and aromatization of n-octane over VMgO catalysts obtained by using different MgO precursors and different precursor treatments).

Our recent publication on the gas-phase non-catalytic ODH of n-hexane show that the rate-determining step is the abstraction of β-hy-drogen by molecular O_2 [41] (N.E. Damoyi H. F.). We proposed that molecular O_2 plays an important role in the radical propagation steps through the intermediates, to produce 1- and 2-hexene and the more reactive %OH and HO_2 radicals. Since our present studies include both molecular O_2 and isolated H_3VO_4, we therefore seek to compare the contribution of H_3VO_4 and O_2 in the activation of n-hexane and radical propagation steps to produce 1- and 2-hexene. Although our modelling is an oversimplification of heterogeneous surface reactions because of the methodology followed, namely, gas-phase calculations on isolated active sites, we believe that the results will be essential in acquiring a theoretical baseline for future potential periodic-DFT calculations of this system. Furthermore, comparisons of the results with those ob-tained in our recent work [41] (N.E. Damoyi H.F.) on gas-phase non-catalytic ODH of n-hexane would be useful, since under certain ex-perimental conditions, gas-phase ODH mechanisms may compete with the catalytic ODH mechanisms. A second study that used a bigger model ($H_4V_2O_7$ as catalyst) is being finalised for publication.

The activation energies ($E^{\#}$), electronic energy (E) and Gibbs energy (G) changes were calculated and these properties facilitate the elucidation of the likely intermediate species involved and the mechanistic pathways followed for the transformation of n-hexane to 1-and 2-hexene.

2. Theoretical methodology

2.1. Computational details

Gas-phase DFT calculations were performed using the Gaussian 09W package [42] (Frisch & et. al.) incorporating the Gausview 5.0 graphics interface. All calculations were performed on a cluster based at the Centre for High Performance Computing (CHPC) in Cape Town, South Africa. All the structures were optimized without constraints and the harmonic vibrational frequencies performed using the B3LYP hy-brid functional, which combines Becke's three-parameter nonlocal hy-brid exchange potential and the nonlocal correlation functional of Lee, Yang and Parr [43] (Becke), [44] (Lee, Yang, & Parr). This functional is known to provide a good description of the potential energy surface (PES) of transition metal-containing compounds [45–47]. The 6–311 + g(d,p) basis set was employed for C, O and H atoms and the V atom described using the relativistic Stuttgart effective core potentials (ECPs) [48] (Dolg, Wedig, Stoll, & Preuss), [49](Martin & Sunder-mann). The transition states (TS) were determined by using relaxed-PES scan techniques on the closed shell and open-shell singlet systems and the laboratory experimental conditions, namely 573, 673 and 773 K, were utilized. The intrinsic reaction coordinate (IRC) calculations in the mass-weighted internal coordinate system, using the algorithm devel-oped by González and Schlegel [50] (Gonzales & Schlegel), [51] (Gonzales & Schlegel), were conducted to confirm the connection of transition states to related minima. The natural bonding orbital (NBO) calculations were performed using the NBO 3.1 program as im-plemented in the Gaussian 09W package and the donor–acceptor in-teractions were analysed based on second order perturbation theory analysis of Fock matrix in NBO basis [52] (Carpenter & Weinhold), [53] (Carpenter & Weinhold, The structure of small molecules and ions).

2.2. Model system

Fig. 1 displays the structure of the selected model of the proposed active site, namely the H_3VO_4 monomeric unit with vanadium in a tetrahedral coordination sphere. This model has been utilized before in DFT modelling studies of similar systems [54](L. Gracia P. G.-N.), [55] (Lei Cheng G. A.). The structure has one V]O bond with vanadium in its highest oxidation state (+5), and the three H atoms are added to balance the −3 charge on the three O atoms. In all calculations the atoms were allowed to relax. Comparisons of some calculated para-meters and vibrational spectra of the model structure with experimental values show that the percentage errors in the calculated V]O bond length is 1% and that of the VeO bond length is 3%. The calculated percentage error for the V]O stretching vibration is 6%. Cartesian coordinates of optimized structures are included with supplementary material.

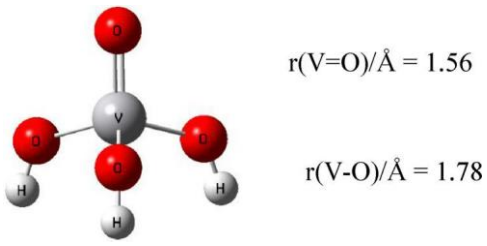

Fig. 1. H_3VO_4 model. B3LYP/6-311 + G(d,p) for H and O atoms, and Stuttgart ECPs for the V atom.

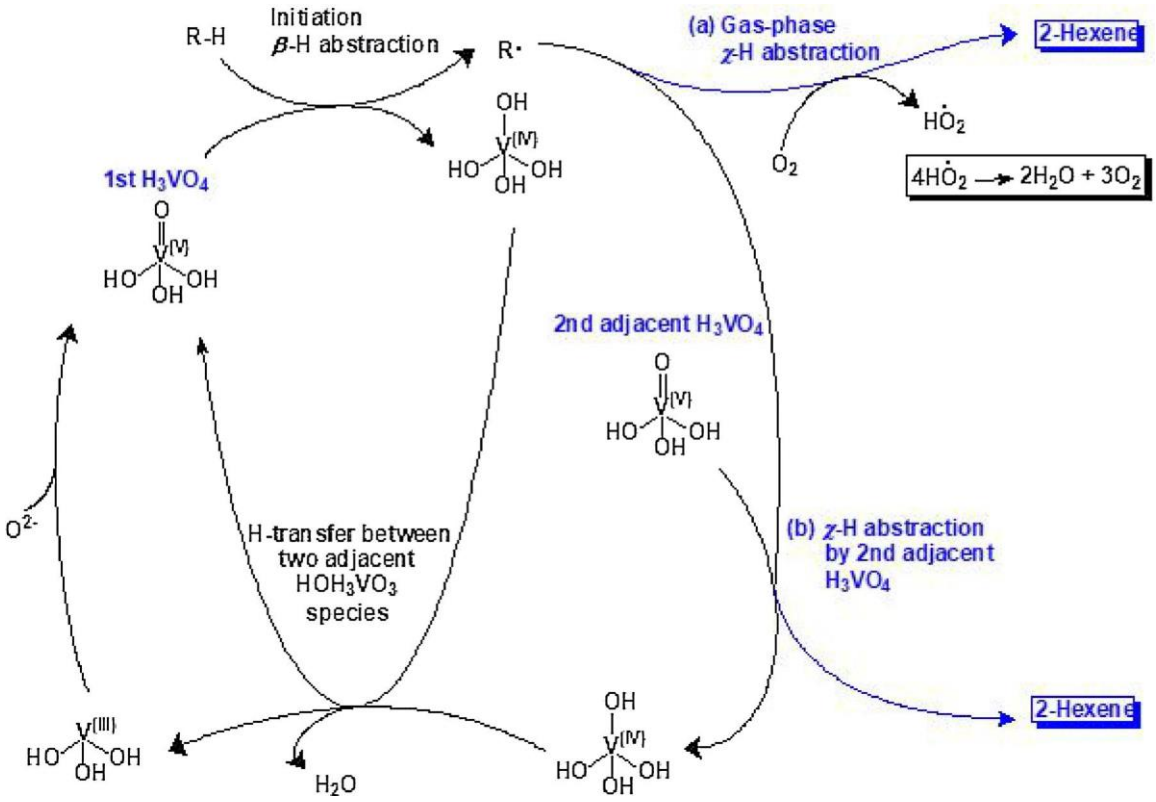

Fig. 2. Proposed reaction scheme, R = C_6H_{13}.

2.3. Reaction scheme for n-hexane to 2-hexene

The proposed reaction scheme for the catalytic (H_3VO_4) ODH re-action of n-hexane to 2-hexene is shown in Fig. 2. Observations from our recent experimental results [56](J. Chetty, accepted.), reflect that only 1- and 2-hexene (no 3-hexene) exist in equilibrium in the reactor over VMgO catalysts, as also suggested by Hoog et al. [57] (Hoog, Herheus, & Zuiderweg). Fig. 2 only indicates the pathway for formation of 2-hexene for clarity purposes.

The rate-determining step involves H-abstraction from the n-hexane chain by the vanadyl O atom in H_3VO_4, leading to a complex inter-mediate, $C_6H_{13}HOH_3VO_3$, and a new VeOeH bond. This is associated with the change in vanadium oxidation state from (V) in H_3VO_4 to (IV) in $C_6H_{13}HOH_3VO_3$. Two pathways that may lead to 2-hexene are (a) the gas-phase γ-H abstraction, where the intermediate fragment (%C_6H_{13} in $C_6H_{13}HOH_3VO_3$) may interact with gas-phase O_2 to produce 2-hexene and a hydroperoxyl radical species (HO_2%), and (b) γ-H abstraction by second H_3VO_4, where a vanadyl O atom abstracts the second γ-H atom to form 2-hexene and another VeOeH bond in HOH_3VO_3. Interaction between the two formed V(IV) species (HOH_3VO_3) may involve dis-proportionation through H-transfer from one entity to another to pro-duce H_2O and regenerate V(V) as H_3VO_4 and also V(III) as H_3VO_3. The radical termination step may occur through disproportionation of the HO_2% radicals, produced in pathway (a) above, into water and oxygen. Finally, the reoxidation of V(III) to V(V) may be achieved through the Mars–van Krevelen mechanism [24](Mars & Van Krevelen) with surface O species.

3. Results

3.1. Activation of n-hexane

The main aim of this study was to characterize the most likely mechanistic steps associated with the interaction of n-hexane and the related intermediates with the model catalyst (H_3VO_4) and O_2 under specific conditions in order to gain insight about the overall mechanism that is followed for the reaction.

The energy profile of the singlet PES for the interaction of n-hexane with H_3VO_4 at 673 K is displayed in Fig. 3 and all the energies are recorded in Table 1. The CeH bond activation through H-abstraction by the vanadyl O (V]O) has been identified as the rate-determining step (RDS) for alkanes ODH to alkenes on V_2O_5 and supported vanadium oxide in several mechanistic studies [58–61]. In our previous theore-tical work on the gas-phase non-catalytic ODH of n-hexane we con-cluded that the RDS is H-abstraction by $^3O_2$, with a barrier height of

$E^{\#}$ = +42.4 kcal/mol [41] (N.E. Damoyi H. F.). In our present work we calculated the RDS as β-hydrogen abstraction by the vanadyl O of H_3VO_4 to produce the intermediate 1 (Int_1–Fig. 3), $C_6H_{13}HOH_3VO_3$. We calculated the activation barrier (TS_1– Fig. 3) with $E^{\#}$ = +27.4 kcal/ mol for this step. A number of authors have also reported on the for-mation of similar radical intermediates that eventually lead to the formation of olefins [54] (L. Gracia P. G.-N.), [15] (Tamara, Yoshida, Ishida, & Kakioka), [62] (Eon, Olier, & Volta). This reaction step is associated with the cleavage of the π-bond in V]O to form a new VeOeH bond and the V centre alters its state from V^{5+} to V^{4+}. The VO bond length simultaneously increases from 1.56 Å in the isolated unit to 1.71 Å in TS1 and 1.78 Å in Int_1. The presence of V^{4+} sites on the partially reduced catalytic surface has been confirmed experimentally for both the unsupported and supported vanadia catalysts [63–65]. Our calculated barrier is comparable to experiments reported by Argyle et al. [61] (Argyle M. D., Chen, Iglesia, & Bell), [66] (Argyle M., Chen, Bell, & Iglesia), who measured the activation barrier for both propane and ethane ODH on alumina-supported vanadia and found both to be +27 kcal/mol. Our results show that intermediate 2 (Int_2– Fig. 3), with the VeC bond, is unlikely to form because of its thermodynamic in-stability with E = +4.8 kcal/mol compared to Int_1 (E = −3.4 kcal/ mol), relative to TS_1.

Fig. 4 displays the propagation steps we explored that lead to 2-

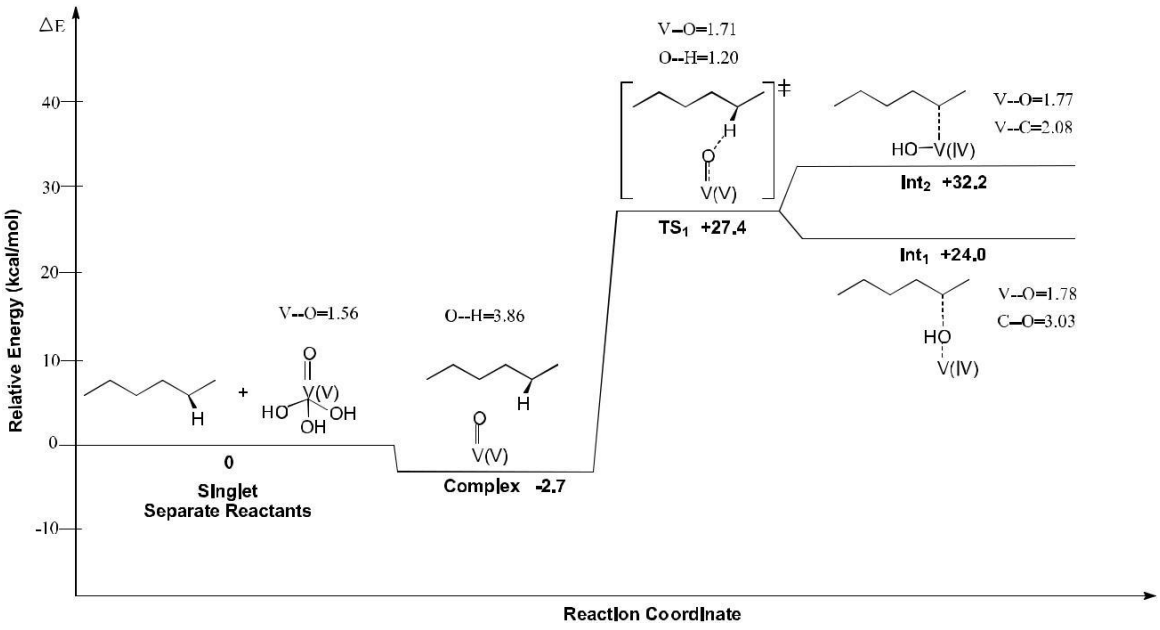

Fig. 3. Zero-point corrected relative electronic energy (E) diagram for activation of n-hexane over H_3VO_4. B3LYP/6-311 + g(d,p) for the C, O and H atoms, and Stuttgart ECPs for the V atom. The indicated bond distances are in Å. Cartesian coordinates of all TSs are provided as supplementary material.

hexene. All the energies, including those for the 1-hexene pathway are recorded in Table 1. The pathway coloured in red indicates the second H-abstraction from the $\%C_6H_{13}$ radical by the OH group within Int_1 to produce 2-hexene, V(III) and H_2O. The calculated barriers are respec-tively, +34.4 (TS_2 – Fig. 4) and +40.3 kcal/mol (TS_5) and the products stabilize to P_1 with E = +5.0 and P_4 = +24.3 kcal/mol for the for-mation of 2- and 1-hexene. In the ODH of n-propane, Hui et al. [64] (Hui Fu) reported reaction barriers (> 30 kcal/mol) for a similar pathway, namely, abstraction of the second H from the same O site as that of the first H abstraction, leading to formation of propene. The authors suggested that this pathway is likely to be hindered by high reaction barriers and they proposed that the second H-abstraction oc-curs on a different O site. In light of this we explored the abstraction of the second H on a different vanadyl O site, to produce 2- and 1-hexene.

The reaction equation for the pathway is: H_3VO_4 + $\%C_6H_{13}$ = HOH_3VO_3 + C_6H_{12}. We calculated barriers of $E^{\#}$ = +0.3 (TS_3 – Fig. 4) and +0.8 kcal/mol (TS_6) for this step and E = −33.5 (P_3) and −30.8 kcal/mol (P_6) for the formation of 2- and 1-hexene, respectively. Our results are in agreement with what was reported by Hui et al. Since gas phase O_2 is another species present in the reaction mixture, we calculated the propagation pathway that involves H-ab-straction from $\%C_6H_{13}$ by O_2. Barrier-less TS_4 (Fig. 4) and TS_7 with the respective values of $E^{\#}$ = −3.0 and −2.9 kcal/mol and E = −14.7 (P_2) and −11.4 (P_5) kcal/mol were calculated for 2- and 1-hexene. In all the above pathways, the formation of the olefins is accompanied by decrease in π-bond-forming CC bond lengths from ~1.5 Å in $\%C_6H_{13}$ to ~1.4 Å in the transition state (TS) and ~1.3 Å in the produced alkene.

Comparisons of energetics for the two likely steps for the second H-abstraction, namely, either from a different vanadyl O site ($E^{\#}$ = +0.3 kcal/mol and E = −33.5 kcal/mol) or from the gas-phase O_2 ($E^{\#}$ = −3.0 kcal/mol and E = −14.7 kcal/mol) for the formation of 2-hexene, indicate that gas phase H-abstraction is slightly more kinetically favourable (by −2.7 kcal/mol), albeit the products formed are less thermodynamically favourable by +18.8 kcal/mol. A relatively large amount of gas phase O_2 in the experimental mixture coupled with low V(V)]O surface areas may lead to the domination of the gas-phase pathway, and the opposite may be true also. Our recent experimental results [56] (J. Chetty, accepted.) for the same catalytic system indicate an increase in selectivity to total dehydrogenation with increase in n-hexane to air ratio, suggesting that the surface site

dehydrogenation reaction is likely to dominate the gas-phase dehy-drogenation reaction. Our modelling results agree with these experi-mental findings as demonstrated by larger negative E value (−33.5 kcal/mol) for the vanadyl O site dehydrogenation reaction re-lative to the gas phase O_2 E value (−14.7 kcal/mol). In our previous results on gas-phase ODH of n-hexane [41] (N.E. Damoyi H. F.), we found that the $\%C_6H_{13}$ radical (Fig. 4) is not likely to undergo in-tramolecular H-elimination to produce 1- or 2-hexene and the H%ra-dical. This is because of the calculated barriers of E# = +38.2 and +36.3 kcal/mol and values of E = +39.5 and +36.5 kcal/mol for the formation of 1- and 2-hexene, respectively, confirming that the path-ways are kinetically and thermodynamically less feasible. However, chemisorption of the $\%C_6H_{13}$ radical on the H_3VO_4 or O_2, rather than H-abstraction, may produce more stable intermediates, $C_6H_{13}VO_4H_3$ and $C_6H_{13}O_2$% respectively, with high barriers for releasing 2-hexene and thereby enabling side-reaction channels, such as complete oxidation to undesired carbon oxides and production of oxygenates [67] (Argyle M. D., Chen, Resini, Krebs, Bell, & Iglesia). Table 1 shows the calculated adsorption energies of the $\%C_6H_{13}$ radical on to the O atoms in H_3VO_4

and O_2 as $E^{\#}$ = −4.9 (TS_8) and +1.9 kcal/mol (TS_9), and E = −46.0 (Int_3) and −28.6 kcal/mol (Int_4), respectively. Clearly, low barriers for both adsorption and H-abstraction processes coupled with large differences in the stabilities of the intermediates suggest that the adsorption and H-abstraction pathways are likely to be driven by thermodynamic terms. This may be the reason why, amongst other products, low yields of less than 20% for 1- and 2-hexene are obtained in our laboratory experiments.

Since the Int_1 fragment, HOH_3VO_3, is not likely to be involved in the second H-abstraction, an accumulation of the OH groups on the surface is likely. Therefore, another pathway for H_2O formation through the coupling of adjacent surface OH groups is feasible, as also suggested by Hui et al. [64] (Hui Fu) in the production of propene through ODH of propane. We therefore investigated the interaction energetics between two adjacent HOH_3VO_3 species. This reaction step pertains to H-transfer from one HOH_3VO_3 species to another to produce H_2O, H_3VO_4 and H_3VO_3 and represents a disproportionation pathway from two V (IV) centres to produce V(III) and V(V) species, followed by reoxidation
of the V(III) to V(V). We calculated an activation barrier with $E^{\#}$ = +3.6 kcal/mol (TS_{10} – Fig. 5) and E = −5.9 kcal/mol (Int_5) for this pathway and the stabilities of H_2O and H_3VO_4 that are produced

Table 1

Relative Energies (E) and Gibbs Free Energies (G) for the reaction of n-hexane with H_3VO_4 to produce 1- and 2-hexene[a]. B3LYP/6-311 + g(d,p) for the C, O and H atoms, and Stuttgart ECPs for the V atom. Cartesian coordinates of all TSs are provided as supplementary material.

Reaction Pathway	E	G		
		573	673	773
Initiation				
s-C_6H_{14} + H_3VO_4	0	0	0	0
s-C_6H_{14} − H_3VO_4 (TS_1)	+27.4	+42.7	+45.8	+48.7
s-TS_1→C_6H_{13} − HO-VO_3H_3 (Int_1)	+24.0 (−3.4)	+32.5 (−10.2)	+34.3 (−11.5)	+36.0 (−12.7)
s-TS_1→C_6H_{13}-VO_3H_3-HO (Int_2)	+32.2 (+4.8)	+51.9 (+9.2)	+55.7 (+9.9)	+59.4 (+10.7)
Propagation from Int_1				
s-C_6H_{13}-HO-VO_3H_3	0	0	0	0
s-Int_1→C_6H_{13}-HO-VO_3H_3 (TS_2): 2-hexene	+34.4	+31.2	+30.8	+30.2
s-Int_1→C_6H_{13}-HO-VO_3H_3 (TS_5): 1-hexene	+40.3	+42.5	+42.9	+42.6
s-TS_2→C_6H_{12} + H_3VO_3 + H_2O (P_1)	+5.0 (−29.4)	−0.6 (−31.8)	−1.5 (−32.3)	−2.5 (−32.7)
s-TS_5→C_6H_{12} + H_3VO_3 + H_2O (P_4)	+24.3 (−16.0)	+17.2 (−25.3)	+16.2 (−26.7)	+14.7 (−27.9)
Propagation from separate H_3VO_4				
d-C_6H_{13} + H_3VO_4	0	0	0	0
d-C_6H_{13} − H_3VO_4 (TS_3): 2-hexene	+0.3	+21.2	+25.2	+29.0
d-C_6H_{13} − H_3VO_4 (TS_6): 1-hexene	+0.8	+22.9	+25.9	+31.3
d-TS_3→C_6H_{12} + HOH_3VO_3 (P_3)	−36.7 (−37.0)	−20.2 (−41.4)	−17.1 (−42.3)	−13.8 (−42.8)
d-TS_6→C_6H_{12} + HOH_3VO_3 (P_6)	−30.8 (−31.6)	−17.2 (−40.1)	−14.5 (−40.4)	−11.8 (−43.1)
Propagation with O_2–H abstraction				
d-C_6H_{13} + O_2	0	0	0	0
d-C_6H_{13} − O_2 (TS_4): 2-hexene	−3.0	+19.7	+23.9	+28.1
d-C_6H_{13} − O_2 (TS_7): 1-hexene	−2.9	+20.0	+24.2	+28.4
d-TS_4→C_6H_{12} + HO_2 (P_2)	−14.7 (−11.7)	−0.6 (−20.3)	+0.7 (−23.2)	+4.8 (−23.3)
d-TS_7→C_6H_{12} + HO_2 (P_5)	−11.4 (−8.5)	+2.3 (−17.7)	+5.5 (−18.7)	+7.7 (−20.7)
C_6H_{13} adsorption on H_3VO_4 and O_2				
d-C_6H_{13} + H_3VO_4 or O_2	0	0	0	0
d-C_6H_{13} − H_3VO_4 (TS_8)	−4.9	+15.5	+17.8	+19.5
d-TS_8→$C_6H_{13}VO_4H_3$ (Int_3)	−46.0 (−41.1)	−14.0 (−29.5)	−16.4 (−34.2)	−18.0 (−37.5)
d-C_6H_{13} − O_2 (TS_9)	+2.6	+37.9	+29.3	+48.0
d-TS_9→$C_6H_{13}O_2$ (Int_4)	−30.2 (−32.8)	−6.7 (−44.6)	−2.4 (−31.7)	+2.0 (−46.0)
Propagation involving $2HOH_3VO_3$				
s-HOH_3VO_3 + HOH_3VO_3	0	0	0	0
s-HOH_3VO_3 − HOH_3VO_3 (TS_{10})	+3.6	+25.2	+29.2	+33.3
s-TS_{10}→H_3VO_3 + H_3VO_4 + H_2O (Int_5)	−5.9 (−9.5)	+12.2 (−13.0)	+15.6 (−13.6)	+19.0 (−14.3)
Reoxidation of H_3VO_3 to H_3VO_4				
t-H_3VO_3 + “surface O”	0	0	0	0
t-H_3VO_3 − “surface O” (TS_{11})	−119.4	−96.1	−52.2	−109.1
t-TS_{11}→H_3VO_4 (P_7)	−239.7 (−120.3)	−220.2 (−124.1)	−216.5 (−164.3)	−213.0 (−103.9)
Termination				
s-HO_2 + HO_2	0	0	0	0
s-HO_2 − HO_2 (TS_{12})	−2.3	+4.9	+5.8	+6.7
s−TS_{12}→2HO + O_2 (Int_6)	−21.1 (−18.8)	−23.4 (−28.3)	−24.1 (−29.9)	−24.9 (−31.6)
t-HO − HO (TS_{13})	−4.7	+8.5	+11.0	+13.6
t-TS_{13}→H_2O + O (Int_7)	−13.0 (−8.3)	−3.2 (−11.7)	−1.3 (−12.3)	+0.7 (−12.9)
t-O − O (TS_{14})	−2.1	+10.7	+13.1	+15.6
t-TS_{14}→O_2 (P_8)	−117.8 (−115.7)	−104.2 (−114.9)	−101.6 (−114.7)	−99.0 (−114.6)

[a] E and G are zero-point corrected electronic energy and Gibbs free energy at standard pressure, relative to separate reactants respectively, in kcal/mol. The energies in parentheses are for the indicated reaction pathways. The temperature is in K and E values are at 673 K. Prefixes s-, d- and t- indicate singlet, doublet and triplet states, respectively.

indicate that the pathway is kinetically and thermodynamically fa-vourable. Termination and reoxidation of H_3VO_3 to H_3VO_4 is likely to proceeds via a Mars–van Krevelen mechanism. We explored separately the adsorption of “surface O” and O_2 on to the V(III) centre and cal-culated a barrier-less energy of activation, $E^{\#}$ = −119.4 kcal/mol (TS_{11} – Fig. 5) for the O^- species (NBO atomic charge = −0.860 – Table 2) and E = −239.7 kcal/mol (P_7) for the formation of H_3VO_4. However, we could not determine the TS for reoxidation with molecular O_2. If the formation of 2-hexene proceeds through gas-phase H-ab-straction by O_2, then the termination step (Fig. 2) may involve dis-proportionation of the produced hydroperoxyl radical to produce H_2O and O_2, as recorded in Table 1 (TS_{12}–TS_{14}) and our previous calcula-tions [41] (N.E. Damoyi H. F.).

We believe that future periodic-DFT calculations that we will en-gage in for this system with a variety of oxide supports will assist in the modifications of the kinetic and thermodynamic terms and as a result reveal the best oxide support for the vanadium oxide catalyst. This is likely because the support may modify the activity of the vanadia monolayer by changing the activation energy of the potentially rate-determining step and affect the selectivity of the active vanadia phase by favouring the formation of the alkene compared to the formation of oxygenated products [30] (Alexopoulos, Reyniers, & Marin). The in-creased/decreased activity of the vanadia monolayer in H-abstraction is well explained by the increase of the chemical hardness above the va-nadyl oxygen (increased proton affinity) and of the Lewis acidity of vanadium (increased electron affinity) upon deposition of the vanadia monolayer on the support [68] (K. Alexopoulos), [69] (M. Calatayud).

3.2. Temperature effects

The laboratory experimental conditions with a temperature range of 573–773 K were included in modelling the reaction. Gibbs free energies of activation ($G^{\#}$) and Gibbs free energies (G) were calculated for all the reaction pathways over the temperature range as indicated in

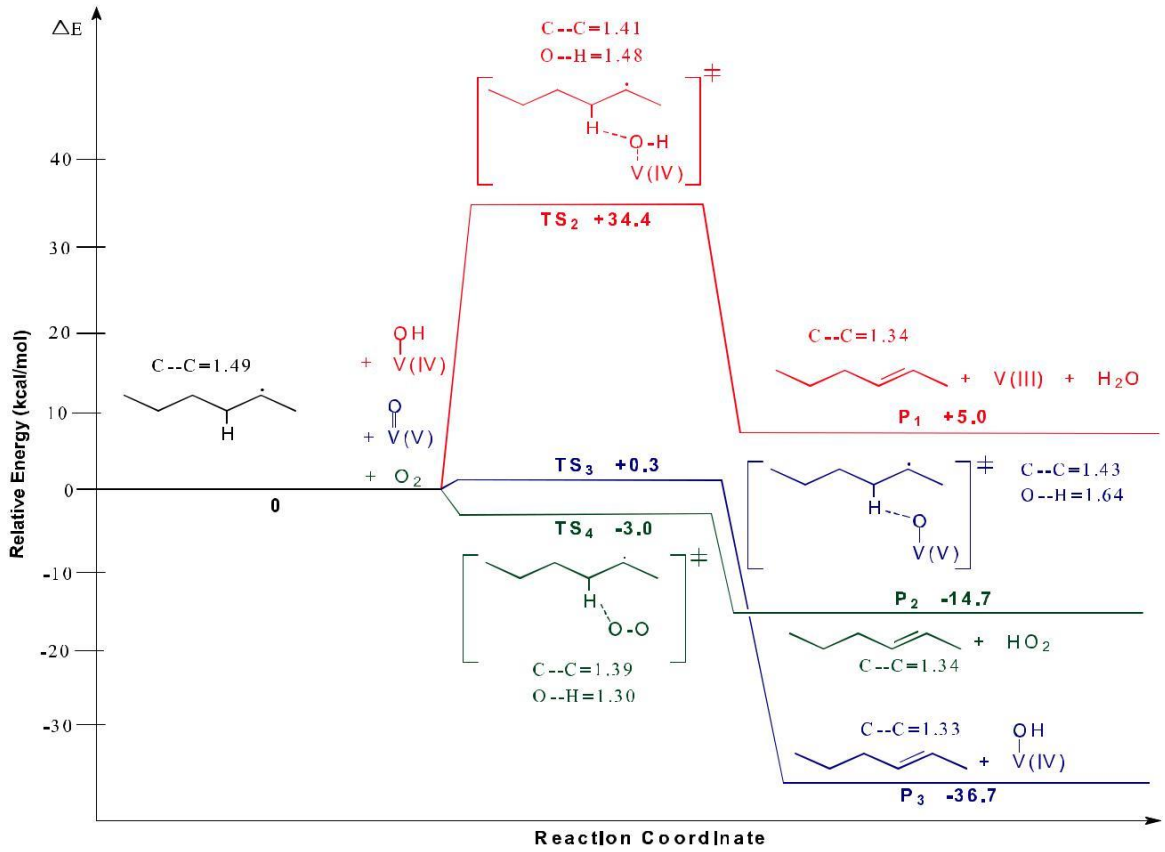

Fig. 4. Zero-point corrected relative electronic energy (E) diagram for propagation pathways for the formation of 2-hexene. The route through TS_2 indicates the kinetically unfavourable pathway for H-abstraction from %C_6H_{13} within Int_1. The routes through TS_3 and TS_4 represent the kinetically and thermodynamically favourable pathways for H-abstraction from a different V(V) centre and gas-phase O_2, respectively. B3LYP/6-311 + g(d,p) for the C, O and H atoms, and Stuttgart ECPs for the V atom. The indicated bond distances are in Å. Cartesian coordinates of all TSs are provided as supplementary material.

Table 1.

For the rate-determining step (TS_1), $G^{\#}$ increases as the tempera-ture increases from 573 to 673 and 773 K. From the $G^{\#}$ values and transition state theory, we calculated the corresponding rates (k) per active site over the three temperatures and obtained the following re-sults, $k(573) = 6.18 \times 10^{-4}\ s^{-1}$, $k(673) = 1.87 \times 10^{-2}\ s^{-1}$ and k (773) = $2.73 \times 10^{-1}\ s^{-1}$. The calculated k(773) per active site is ap-proximately three orders of magnitude and one order of magnitude greater than the values at 573 and 673 K, respectively. This indicates that the rate-determining step is kinetically more favourable at 773 K. A similar trend is observed in $G^{\#}$ values for all the propagation pathways where the reactions become more faster as the temperature increases.

The lowest calculated G value for the rate-determining step is +32.5 kcal/mol for the formation of Int_1 at 573 K. The G values at 673 and 773 K are +34.3 and +36.0 kcal/mol, respectively. Our calcula-tions from the attached supplementary material show that the enthalpy (H = +22.0 kcal/mol) and entropy magnitude (T S = −10.5 kcal/ mol) contributions are lowest at 573 K and slightly highest at 773 K (H = +23.2 and T S = −12.8 kcal/mol). Furthermore, at all tem-peratures the H contributions are the dominant factors to the G va-lues and are approximately two (2) times the magnitude values of T S. Therefore, the specified temperature range is likely to play a minimal role in the thermodynamic formation of Int_1 in the rate-determining step. A similar trend is also observed in G values for all the propa-gation pathways where there are small differences in the thermo-dynamic factors at all temperatures.

Our group experimental results [56] (J. Chetty, accepted.) using the same catalyst system under similar conditions show that the total de-hydrogenation selectivity increases from 573 to 773 K. Our modelling results concur with experiments in that the formation of 1- and 2-hexene from ODH of n-hexane by H-abstraction with surface H_3VO_4, followed by the second H-abstraction from either a different surface H_3VO_4 or from gas-phase O_2, is likely to be relatively more kinetically favourable at 773 K and thermodynamically favourable at all the spe-cified temperatures.

3.3. Natural bond orbital analyses

NBO calculations [52] (Carpenter & Weinhold), [53] (Carpenter & Weinhold, The structure of small molecules and ions) were conducted on the selected transition states of the most likely pathways at the B3LYP/6 − 311 + G(d,p) level. Fig. 6 displays the TSs and the asso-ciated highest occupied NBOs (HONBOs) representing the donor orbi-tals, and the lowest unoccupied NBOs (LUNBOs) representing acceptor orbitals. The calculation separates the system into a number of frag-ments based on largest interatomic distances. Electron density shifts are calculated within and amongst the fragments. The largest electron density shifts are estimated as delocalization with highest second order stabilization energies, E(2) values, which indicate regions of high ac-tivity in the system. For each TS, the atomic charges of the interacting atoms, the NBOs and the largest stabilization energies are recorded in Table 2.

The rate-determining step (TS_1) is associated with the H-abstraction by vanadyl O from the H_3VO_4 unit and the corresponding donor orbital is the Lewis-type highest occupied NBO (HONBO) that is a C s(7.2%) p (92.8%) hybrid-type character. The acceptor orbital is the non-Lewis-type lowest unoccupied NBO (LUNBO) that is H s-type character. The spatial orientation of the two interacting species facilitates maximum overlap of the orbitals. The stabilization energy involved with the transfer of electron density is +272.4 kcal/mol, indicating a strong

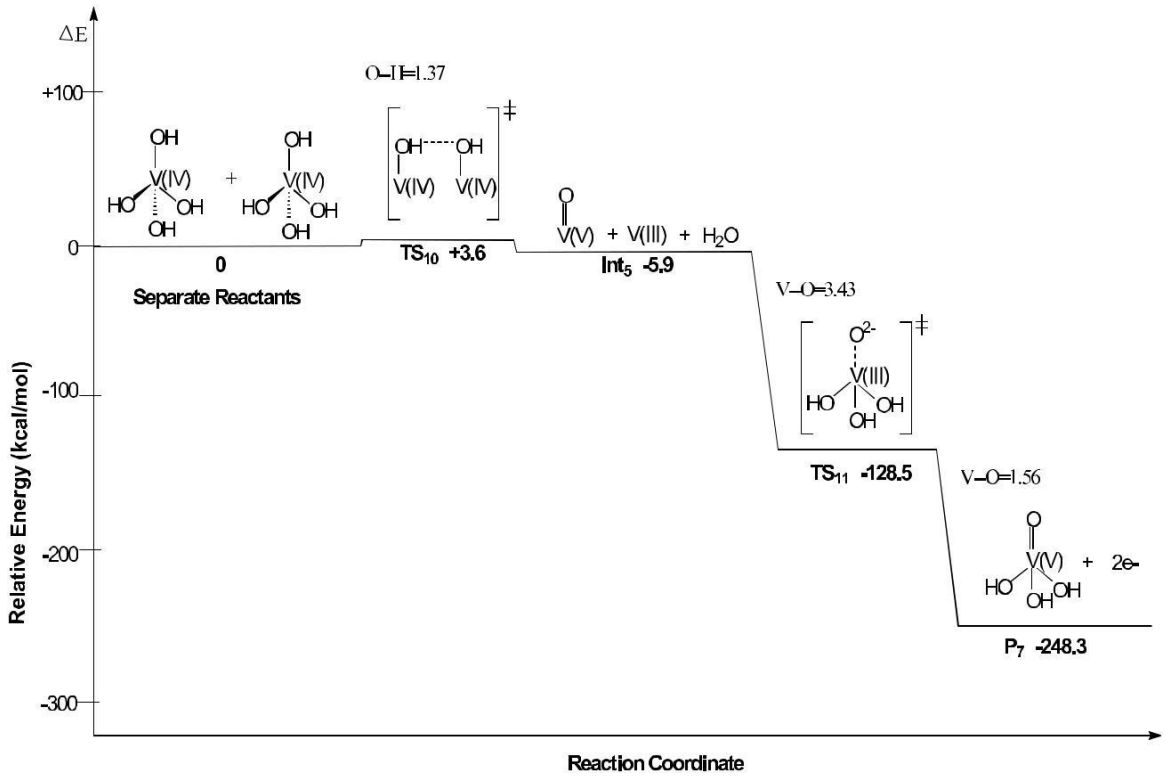

Fig. 5. Zero-point corrected relative electronic energy (E) diagram for disproportionation of two V(IV) centres to produce V(III) and V(V) centres, followed by reoxidation of V(III) to (V) by O^{2-}. B3LYP/6-311 + g(d,p) for the C, O and H atoms, and Stuttgart ECPs for the V atom. The indicated bond distances are in Å. Cartesian coordinates of all TSs are provided as supplementary material.

Table 2

Selected NBO atomic charges, HONBO and LUNBO orbital types, and orbital energies for the TSs of the n-hexane to 1- and 2-hexene pathways. B3LYP/6-311 + g(d,p) for all the atoms. Cartesian coordinates of all TSs are provided as supplementary material.

TS	Atomic charges on interacting atoms	HONBO type (donor)	LUNBO type (donor)	Stabilization Energy (kcal/mol)
1	C = −0.336 H = +0.324 O = −0.512	C s(7.2%) p(92.8%) nonbonding hybrid	H s-type antibonding	+272.4
3 (2-hexene)	C = −0.505 H = +0.327 O = −0.492	O s(79.9%) p(20.3%) nonbonding hybrid	H s and C s(18.6%) p(81.4%) antibonding hybrid	+4.86
4 (2-hexene)	C = −0.387 H = +0.192 O = −0.408	O s(13.3%) p(86.7%) nonbonding hybrid	H s and C s(13.0%) p(87.0%) antibonding hybrid	+45.9
6 (1-hexene)	C = −0.684 H = +0.324 O = −0.491	O s(80.0%) p(20.0%) nonbonding hybrid	H s and C s(20.7%) p(79.3%) antibonding hybrid	+7.86
7 (1-hexene)	C = −0.478 H = +0.360 O = −0.225	O s(13.1%) p(86.9%) nonbonding hybrid	H s and C s(11.6%) p(88.4%) antibonding hybrid	+42.1
10	O = −0.926 H = +0.500 O = −0.650	O s(16.3%) p(83.7%) nonbonding hybrid	H s and O s(8.5%) p(91.5%) antibonding hybrid	+35.4
11	O = −0.860 V = +0.619	O s(7.9%) p(92.1%) nonbonding	V s(12.1%) p(83.9%) d(4.0%) antibonding hybrid	+1.87

interaction between the two orbitals. The calculated atomic charges indicate a stronger interaction between the O (-0.512) and H (+0.324) as compared to C (−0.336) and H (+0.324). The pathway for the second H-abstraction through a different V site to produce 2-hexene (TS_3) has donor-acceptor orbital characters that are O s(79.7%) p (20.3%) nonbonding and H s and C s(18.6%) p(81.4%) antibonding. The stabilization energy is +4.86 kcal/mol and the charges on the in-teracting atoms are H (+0.327), C (−0.505) and O (−0.492). The donor and acceptor orbitals describing the propagation pathway bar-riers for the formation of 2-hexene (TS_4) through H-abstraction by gas-phase O_2 are the O s(13.3%) p(86.7%) nonbonding hybrid to the H s and C s(11.6%) p(88.4%) antibonding hybrid. The calculated energy is +45.9 kcal/mol. The distribution of atomic charges on interacting atoms follows the same trend with negative charges on C (−0.387) and O (−0.408) atoms and a positive charge on the H (+0.192) atom.

Similar orbitals, atomic charges and comparable orbital stabilization energies were obtained for the 1-hexene pathways, as shown in Table 2 (TS_3 for 2-hexene and TS_6 for 1-hexene, TS_4 for 2-hexene and TS_7 for 1-hexene).

The donor-acceptor orbitals for the disproportionation pathway (H-transfer) of two HOH_3VO_3 to produce H_2O, H_3VO_3 and H_3VO_4 (TS_{10}) are O s(16.3%) p(83.7%) nonbonding hybrid and H s and O s(8.5%) p (91.5%) antibonding hybrid, respectively, with a stabilization energy of +35.4 kcal/mol. The positive charge is on the H atom (+0.500) and the charge on the O atom that releases the H atom is −0.650 and that on the O atom that receives the H atom is −0.926, indicating a stronger interaction between O and H leading to a new OH bond. Lastly, the calculated orbital stabilization energy for reoxidation of V(III) to V(V) through TS_{11} is +1.87 kcal/mol. Examination of the total electron distribution in the TS shows that there are also shifts of electron density

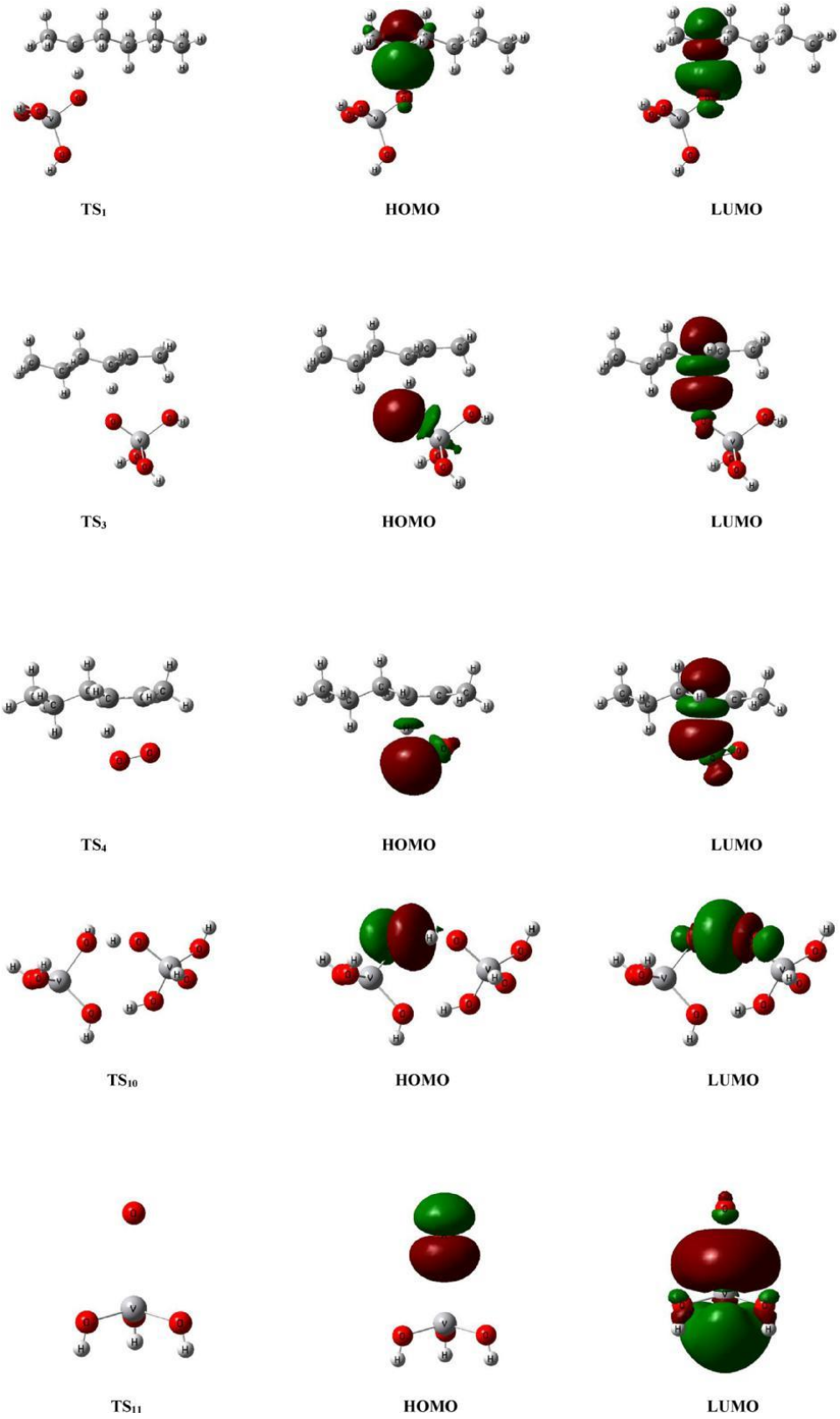

Fig. 6. Selected TS structures and the NBO calculated frontier orbitals for the likely mechanistic pathway for the formation of 2-hexene. The orbital lobes are oriented for better clarity in each case and correspond to the reaction coordinate. B3LYP/6-311 + g(d,p) for all the atoms. Cartesian coordinates of all TSs are provided as supplementary material.

between other O atoms and the V atom in H_3VO_3, which facilitate the formation of a vanadyl bond in H_3VO_4. The delocalization of electron density amongst all the atoms in H_3VO_3 explains the low stabilization energy (+1.87 kcal/mol) in the TS. The NBO atomic charges show the largest negative charge on O atom (−0.860) involved in the TS with the V atom (+0.619).

4. Conclusions

DFT methods have been used to investigate the activity of the tet-rahedral monomeric H_3VO_4 structure for n-hexane ODH. From our calculations we have used kinetic and thermodynamic arguments combined with the NBO qualitative analyses in terms of atomic charges, HOMO and LUMO interactions/delocalisation that show the largest second order stabilization energies, E(2) values, to propose the fol-lowing mechanistic pathways for the reaction,

Initiation:

$$C_6H_{14} + H_3VO_4 = \%C_6H_{13} + HOH_3VO_3$$

n-hexane, H_3VO_4 and O_2 are the only species present initially. The rate-determining step is β-H abstraction from n-hexane by vanadyl O in H_3VO_4 to produce the $\%C_6H_{13} + HOH_3VO_3$ complex intermediate. This step has a barrier of $E^{\#}$ = +27.4 kcal/mol (TS_1). This acti-vation energy is comparable to the experimental value reported by Argyle et al. [61] (Argyle M. D., Chen, Iglesia, & Bell), [66] (Argyle M., Chen, Bell, & Iglesia) for both propane and ethane ODH on alumina-supported vanadia (+27.0 kcal/mol). As expected, our calculated value is also lower than the β-H abstraction by O_2 ($E^{\#}$ = +42.4 kcal/mol) obtained in our previous work on gas-phase ODH. The intermediate stabilizes with E = −3.4 kcal/mol, relative to the transition state (Fig. 3).

Propagation on a different H_3VO_4 site:

$$\%C_6H_{13} + H_3VO_4 = C_6H_{12} + HOH_3VO_3$$

The second γ-H abstraction from the $\%C_6H_{13}$ radical produces 2-hexene and the second HOH_3VO_3 species. This step has $E^{\#}$ = +0.3 kcal/mol (TS_3) and the products stabilize to E = −33.5 kcal/mol, relative to separate reactants. The $E^{\#}$ and E values suggests that the formation of 2-hexene is likely to pro-ceed on a different H_3VO_4 site. This is because we calculated higher activation barriers ($E^{\#}$ > 30 kcal/mol) for the abstraction of the second H atom on the same V site as abstraction of the first H atom (Fig. 4).

Propagation by O_2:

$$\%C_6H_{13} + O_2 = C_6H_{12} + HO_2\%$$

In competition with the previous pathway for the second γ-H ab-straction from the $\%C_6H_{13}$ radical, is the likely involvement of gas-phase O_2, with the products being 2-hexene and the HO_2%radical. This is a barrier-less step with $E^{\#}$ = −3.0 kcal/mol (TS_4) and E = −14.7 kcal/mol, relative to separate reactants (Fig. 4).

Both the propagation pathways may lead to 2-hexene. The chosen pathway is likely to depend on the relative amount of gas-phase O_2 and the surface area of H_3VO_4 sites at any given time.

Disproportionation:

$$HOH_3VO_3 + HOH_3VO_3 = H_3VO_3 + H_3VO_4 + H_2O$$

If the formation of 2-hexene is achieved through propagation on a different H_3VO_4 site, to also produce the HOH_3VO_3 species, then disproportionation of the two HOH_3VO_3 species would follow. This step has a barrier with $E^{\#}$ = +3.6 kcal/mol (TS_{10}) and a stabilization en-ergy of E = −9.5 kcal/mol, relative to TS, for the formation of the products (Fig. 5).

Reoxidation and Termination:

$$H_3VO_3 + \text{surface}\quad O = H_3VO_4$$

$$2HO_2\% = 2HO\% + O_2$$

$$2OH\% = H_2O + O$$

$$2O = O_2$$

The reoxidation of V(III) to V(V) with "surface O" (NBO atomic charge = −0.860) is achieved through a barrier-less height with $E^{\#}$ = −119.4 kcal/mol (TS_{11}) and the produced H_3VO_4 stabilization energy of E = −120.3 kcal/mol, relative to TS. If the formation of 2-hexene is achieved through propagation by gas-phase O_2, then the produced HO_2% radicals disproportionate stepwise to produce O_2 and H_2O with barrier-less energies of $E^{\#}$ = −2.3 (TS_{12}), −4.7 (TS_{13}) and −2.1 kcal/mol (TS_{14}). The associated values of E are −21.1, −13.0 and −117.8 kcal/mol, relative to separate reactants, respectively (Table 1).

A subsequent study that used a bigger model ($H_4V_2O_7$ as catalyst) is being finalised for publication.

Acknowledgments

This work was supported by the NRF, SASOL and Johnsson Matthey. We would like to thank the Centre for High Performance Computing (CHPC) in Cape Town, South Africa, for providing the computational resources necessary to conduct this work.

References

[1] F. Ogliaro, N. Harris, S. Cohen, M. Filatov, S.P. De Visser, S. Shaik, A model 're-bound' mechanism of hydroxylation by cytochrome P450: Stepwise and effectively concerted pathways, and their reactivity patterns, J. Am. Chem. Soc. 122 (2000) 8977–8989.

[2] D.K. Bohme, H. Schwarz, Gas-phase catalysis by atomic and cluster metal ions: the ultimate single-site catalysts, Angew. Chem. Int. Ed. 44 (2005) 2336–2354.

[3] K.A. Zemski, D.R. Justes, R.C. Bell, A.W. Castleman, Reactions of niobium and tantalum oxide cluster cations and anions with n-butane, J. Phys. Chem. A 105 (2001) 4410–4417.

[4] I.P. Belomestnykh, E.A. Skrigan, N.N. Rozhdestvenskaya, G.V. Isaguliants, New preparation methods of multicomponent oxide vanadium systems for oxidative dehydrogenation of alkanes, alkylaromatic and alkylheterocyclic compounds, Stud. Surf. Sci. Catal. 72 (1992) 453–460.

[5] H. Kung, M. Kung, Oxidative dehydrogenation of alkanes over vanadium-magne-sium-oxides, Appl. Catal. A 157 (1997) 105–116.

[6] J. Dobler, M. Pritzsche, J. Sauer, Oxidation of methanol to formaldehyde on sup-ported vanadium oxide catalysts compared to gas phase molecules, J. Am. Chem. Soc. 127 (2005) 10861–10868.

[7] A. Goodrow, A.T. Bell, A theoretical investigation of the selective oxidation of methanol to formaldehyde on isolated vanadate species supported on silica, J. Phys. Chem. C 111 (2007) 14753–14761.

[8] E.A. Elkhalifa, H.B. Friedrich, Oxidative dehydrogenation of n-octane using vana-dium-magnesium oxide catalysts with different vanadium loadings, Appl. Catal. A 373 (2010) 122–131.

[9] N.U. Zhanpeisov, A density functional theory study of the oxidation of methanol to formaldehyde over vanadia supported on silica, titania and zirconia, Res. Chem. Intermed. 30 (2004) 133–141.

[10] J.L. Bronkema, D.C. Leo, A.T. Bell, Mechanistic studies of methanol oxidation to formaldehyde on isolated vanadate sites supported on high surface area anatase, J. Phys. Chem. C 111 (2007) 14530–14540.

[11] L. Burcham, L. Briand, I. Wachs, Quantification of active sites for the determination of methanol oxidation turn-over frequencies using methanol chemisorption and in situ infrared techniques. 1. Supported metal oxide catalysts, Langmuir 17 (2001) 6164–6174.

[12] X. Rozanska, R. Fortrie, J. Sauer, Size-dependent catalytic activity of supported vanadium oxide species: oxidative dehydrogenation of propane, J. Am. Chem. Soc. 136 (2014) 7751–7761.

[13] X. Rozanska, E.V. Kondratenko, J. Sauer, Oxidative dehydrogenation of propane: differences between N2O and O2 in the reoxidation of reduced vanadia sites and consequences for selectivity, J. Catal. 256 (2008) 84–94.

[14] M.M. Islam, D. Costa, M. Calatayud, F. Tielens, Characterization of supported

vanadium oxide species on silica: a periodic DFT investigation, J. Phys. Chem. C 113 (2009) 10740–10746.
[15] K. Tamara, S. Yoshida, S. Ishida, H. Kakioka, Spectroscopic studies of catalysis by vanadium pentoxide, Bull. Chem. Soc. Jpn. 41 (1968) 2840–2845.
[16] C.L. Pieck, M.A. Bañares, J.L.G. Fierro, Propane oxidative dehydrogenation on VOx/ZrO2 catalysts, J. Catal. 224 (2004) 1–7.
[17] H. Kung, Oxidative dehydrogenation of light (C2 to C4) alkanes, Adv. Catal. 40 (1994) 1–38.
[18] T. Balsko, J.M. Lopez-Nieto, Oxidative dyhydrogenation of short chain alkanes on supported vanadium oxide catalysts, Appl. Catal. A 157 (1997) 117–142.
[19] S. Sugiyama, Y. Iozuka, E. Nitta, H. Hayashi, J.B. Moffat, Role of tetra-chloromethane as a gas-phase additive in the oxidative dehydrogenation of propane over cerium oxide, J. Catal. 189 (2000) 233–237.
[20] F. Arena, F. Frusteri, A. Parmaliana, G. Martra, S. Coluccia, Oxidative dehy-drogenation of propane on supported V2O5 catalysts: role of redox and acid-base properties, Stud. Surf. Sci. Catal. 119 (1998) 665–670.
[21] Y.M. Liu, Y. Cao, N. Yi, W.L. Feng, W.L. Dai, S.R. Yan, H.Y. He, K.N. Fan, Vanadium oxide supported on mesoporous SBA-15 as highly selective catalysts in the oxidative dehydrogenation of propane, J. Catal. 224 (2004) 417–428.
[22] E.A. Elkhalifa, H.B. Friedrich, On the effect of hydrocarbon/oxygen ratios during the dehydrogenation of n-octane over a VMgO catalyst, Catal. Lett. 141 (2011) 554–564.
[23] F. Cavani, F. Trifiro, Selective oxidation of light alkanes: interaction between the catalyst and the gas phase on different classes of catalytic materials, Catal. Today 51 (1999) 561–580.
[24] P. Mars, D.W. van Krevelen, Oxidations carried out by means of vanadium oxide catalysts, Chem. Eng. Sci. 3 (1954) 41–59.
[25] A. Andersson, An oxidized surface state model of vanadium oxides and its appli-cation to catalysis, J. Solid State Chem. 42 (1982) 263–275.
[26] K. Mori, A. Miyamoto, Y. Murakami, Catalytic reactions on well-characterized va-nadium oxide catalysts. 4. Oxidation of butane, J. Phys. Chem. 89 (1985) 4265–4269.
[27] S.T. Oyama, Adsorbate bonding and the selection of partial and total oxidation pathways, J. Catal. 128 (1991) 210–217.
[28] K.D. Chen, A.T. Bell, E. Iglesia, The Relationship between the electronic and redox properties of dispersed metal oxides and their turnover rates in oxidative dehy-drogenation reactions, J. Catal. 209 (2002) 35–42.
[29] Y. Liu, Z. Geng, Y. Wang, J. Liu, X. Hou, DFT studies for activation of CeH bond in methane by gas-phase Rhn+ (n = 1 − 3), Comput. Theor. Chem. 1015 (2013) 52 –63.
[30] K. Alexopoulos, M. Reyniers, G.B. Marin, Reaction path analysis of propane selec-tive oxidation over V2O5 and V2O5/TiO2, J. Catal. 289 (2012) 127–139.
[31] E. Kurnaz, M.F. Fellah, I. Onal, A density functional theory study of C-H bond ac-tivation of methane on a bridge site of M-O-M-ZSM-5 Clusters (M = Au, Ag Fe and Cu), Microporous Mesoporous Mat. 138 (2011) 68–74.
[32] M. Witko, Oxidation of hydrocarbons on transition metal oxide catalysts − quantum chemical studies, J. Mol. Catal. 70 (1991) 277–333.
[33] F. Ruette, Quantum Chemistry Approaches to Chemisorption and Heterogeneous Catalysis, Kluwer Academic Publishers, Boston, 1992.
[34] R.A. van Santen, M. Neurock, Concepts in theoretical heterogeneous catalytic re-activity, Catal. Rev. Sci. Eng. 37 (1995) 557–698.
[35] G.A. Somorjai, Y.M. Li, Major successes of theory and experiment-combined studies in surface chemistry and heterogeneous catalysis, Top. Catal. 53 (2010) 311–325.
[36] H.B. Friedrich, N. Govender, M.R. Mathebula, The effect of voids and dilution on n-hexane oxidation over a VMgO catalyst, Appl. Catal. A 297 (2006) 81–89.
[37] B. Pillay, M.R. Mathebula, H.B. Friedrich, The oxidative dehydrogenation of n-hexane over Ni–Mo–O catalysts, Appl. Catal. A 361 (2009) 57–64.
[38] V.D.B.C. Dasireddy, S. Singh, H.B. Friedrich, Activation of n-octane using vanadium oxide supported on alkaline earth hydroxyapatites, Appl. Catal. A 456 (2013) 105–117.
[39] E.A. Elkhalifa, H.B. Friedrich, Oxidative dehydrogenation of n-octane using vana-dium-magnesium oxide catalysts with different vanadium loadings, Appl. Catal. A 373 (2010) 122–131.
[40] E.A. Elkhalifa, H.B. Friedrich, Oxidative dehydrogenation and aromatization of n-octane over VMgO catalysts obtained by using different MgO precursors and dif-ferent precursor treatments, J. Mol. Catal. A: Chem. 392 (2014) 22–30.
[41] N.E. Damoyi, H.B. Friedrich, H.G. Kruger, D. Willock, Density functional theory studies of the uncatalysed gas-phase oxidative dehydrogenation conversion of n-hexane to hexenes, Comput. Theor. Chem. 1114 (2017) 153–164.
[42] M.J. Frisch, G.W. Trucks, H.B. Schlegel, G.E. Scuseria, M.A. Robb, J.R. Cheeseman, G. Scalmani, V. Barone, B. Mennucci, G.A. Petersson, H. Nakatsuji, M. Caricato, X. Li, H.P. Hratchian, A.F. Izmaylov, J. Bloino, G. Zheng, J.L. Sonnenberg, M. Hada, M. Ehara, K. Toyota, R. Fukuda, J. Hasegawa, M. Ishida, T. Nakajima, Y. Honda, O. Kitao, H. Nakai, T. Vreven, J.A. Montgomery, J.E. Peralta, F. Ogliaro, M. Bearpark, J.J. Heyd, E. Brothers, K.N. Kudin, V.N. Staroverov, R. Kobayashi, J. Normand, K. Raghavachari, A. Rendell, J.C. Burant, S.S. Iyengar, J. Tomasi, M. Cossi, N. Rega, N.J. Millam, M. Klene, J.E. Knox, J.B. Cross, V. Bakken, C. Adamo, J. Jaramillo, R. Gomperts, R.E. Stratmann, O. Yazyev, A.J. Austin, R. Cammi, C. Pomelli, J.W. Ochterski, R.L. Martin, K. Morokuma, V.G. Zakrzewski, G.A. Voth, P. Salvador, J.J. Dannenberg, S. Dapprich, A.D. Daniels, Ö. Farkas, J.B. Foresman, J.V. Ortiz, J. Cioslowski, D.J. Fox, Gaussian 09, Revision B.01, Gaussian, Inc, Wallingford, 2010.
[43] A.D. Becke, Density functional thermochemistry III – the role of exact exchange, J. Chem. Phys. 98 (1993) 5648–5652.
[44] C. Lee, W. Yang, R.G. Parr, Development of the Colle-Salvetti correlation energy formula into a functional of the electron density, Phys. Rev. B: Condens. Matter 37 (1988) 785–789.
[45] J. Oxgaard, R.A. Periana, W.A. Goddard, Mechanistic analysis of hydroarylation catalysts, J. Am. Chem. Soc. 126 (2004) 11658–11665.
[46] D. Benitez, W.A. Goddard, The isomerization equilibrium between cis and trans chloride ruthenium olefin metathesis catalysts from quantum mechanics calcula-tions, J. Am. Chem. Soc. 127 (2005) 12218–12219.
[47] J.A. Keith, J. Oxgaard, W.A. Goddard, Inaccessibility of beta-hydride elimination from −OH functional groups in Wacker-type oxidation, J. Am. Chem. Soc. 128 (2006) 3132–3133.
[48] M. Dolg, U. Wedig, H. Stoll, H. Preuss, Energy-adjusted ab initio pseudopotentials for the first row transition elements, J. Chem. Phys. 86 (1987) 866–872.
[49] J.M.L. Martin, A. Sundermann, Correlation consistent valence basis sets for use with the Stuttgart-Dresden-Bonn relativistic effective core potentials: the atoms Ga-Kr and In-Xe, J. Chem. Phys. 114 (2001) 3408–3420.
[50] C. Gonzales, H.B. Schlegel, An improved algorithm for reaction path following, J. Chem. Phys. 90 (1989) 2154–2161.
[51] C. Gonzales, H.B. Schlegel, Reaction path following in mass-weighted internal co-ordinates, J. Phys. Chem. 94 (1990) 5523–5527.
[52] J.E. Carpenter, F. Weinhold, Analysis of the geometry of the hydroxymethyl radical by the different hybrids for different spins natural bond orbital procedure, J. Mol. Struct. THEOCHEM 169 (1988) 41–62.
[53] J.E. Carpenter, F. Weinhold, The natural bond orbital Lewis structure concept for molecules, radicals, and radical ions, in: R. Naaman, Z. Vager (Eds.), The Structure of Small Molecules and Ions, 1988, pp. 227–236 (Plenum N.Y).
[54] L. Gracia, P. González-Navarrete, M. Calatayud, J. Andrés, A DFT study of methanol dissociation on isolated vanadate groups, Catal. Today 139 (2008) 214–220.
[55] L. Cheng, G.A. Ferguson, S.A. Zygmunt, L.A. Curtiss, Structure-activity relationships for propane oxidative dehydrogenation by anatase-supported vanadium oxide monomers and dimers, J. Catal. 302 (2013) 31–36.
[56] J. Chetty, V.D.B.C. Dasireddy, S. Singh, H.B. Friedrich, The oxidative aromatization of n-hexane over VMgO catalysts, Reac. Kinet. Mech. Catal. 120 (2017) 307–321.
[57] H. Hoog, J. Herheus, F.J. Zuiderweg, Investigations into the cyclisation (ar-omatisation) of aliphatic hydrocarbons, Trans. Faraday Soc. 35 (1939) 993–1006.
[58] X. Rozanska, R. Fortrie, J. Sauer, Oxidative dehydrogenation of propane by monomeric vanadium oxide sites on silica support, J. Phys. Chem. C 111 (2007) 6041–6050.
[59] M. Cheng, K. Chenoweth, J. Oxgaard, A. van Duin, W. Goddard, Single-site vanadyl activation functionalization, and reoxidation reaction mechanism for propane oxi-dative dehydrogenation on the cubic V4O10 cluster, J. Phys.Chem. C 111 (2007) 5115–5127.
[60] K.D. Chen, A.T. Bell, E. Iglesia, Kinetic isotopic effects in oxidative dehydrogenation of propane on vanadium oxide catalysts, J. Catal. 192 (2000) 197–203.
[61] M.D. Argyle, K. Chen, E. Iglesia, A.T. Bell, Effect of catalyst structure on oxidative dehydrogenation of ethane and propane on alumina-supported vanadia, J. Catal. 208 (2002) 139–149.
[62] J.G. Eon, R. Olier, J.C. Volta, Oxidative dehydrogenation of propane on γ-Al2O3 supported vanadium oxides, J. Catal. 145 (1994) 318–326.
[63] K. Devriendt, H. Poelman, L. Fiermans, G. Creten, G.F. Froment, Angular resolved XPS applied to V2O5-based catalysts, surf, Sci 352–354 (1996) 750–754.
[64] F. Hui, L. Zhi-Pan, L. Zhen-Hua, W. Wen-Ning, F. Kang-Nian, Periodic density functional theory study of propane oxidative dehydrogenation over V2O5(001) surface, J. Am. Chem. Soc. 128 (2006) 11114–11123.
[65] J. Sauer, J. Döbler, Structure and reactivity of V2O5: bulk solid, nanosized clusters, species supported on silica and alumina, cluster cations and anions, Dalton Trans. (2004) 3116–3121.
[66] M.D. Argyle, K.D. Chen, A.T. Bell, E. Iglesia, Ethane oxidative dehydrogenation pathways on vanadium oxide catalysts, J. Phys. Chem. B 106 (2002) 5421–5427.
[67] M.D. Argyle, K. Chen, C. Resini, C. Krebs, A.T. Bell, E. Iglesia, Extent of reduction of vanadium oxides during catalytic oxidation of alkanes measured by in-situ UV-visible spectroscopy, J. Phys. Chem. B 108 (2004) 2345–2353.
[68] K. Alexopoulos, P. Hejduk, M. Witko, M.-F. Reyniers, G.B. Marin, Theoretical study of the effect of (001) TiO2 anatase support on V2O5, J. Phys. Chem. C 114 (2010) 3115–3130.
[69] M. Calatayud, F. Tielens, F. De Proft, Reactivity of gas-phase, crystal and supported V2O5 systems studied using density functional theory based reactivity indices, Chem. Phys. Lett. 456 (2008) 59–63.